Supplementary Information

Breaking the activity-stability trade-off in acidic oxygen evolution reaction via steering charge-compensation mechanisms in RuO_2

Zhijian Li[aξ], Huaipeng Pang[bξ], Yifan Shao[a], Deqing Kong[a], Hao Zhou[a], Yijun Yang[a] and Xi Wang[a]*

[a] Key Laboratory of Luminescence and Optical Information, Ministry of Education, School of Physical Science and Engineering, Beijing Jiaotong University, Beijing 100044, P. R. China.
[b] School of Materials Science and Engineering, Ocean University of China, Qingdao, 266404, China.
[ξ]These authors contributed equally to this work.

*Corresponding contributor. E-mail: xiwang@bjtu.edu.cn

† Electronic supplementary information (ESI) available.

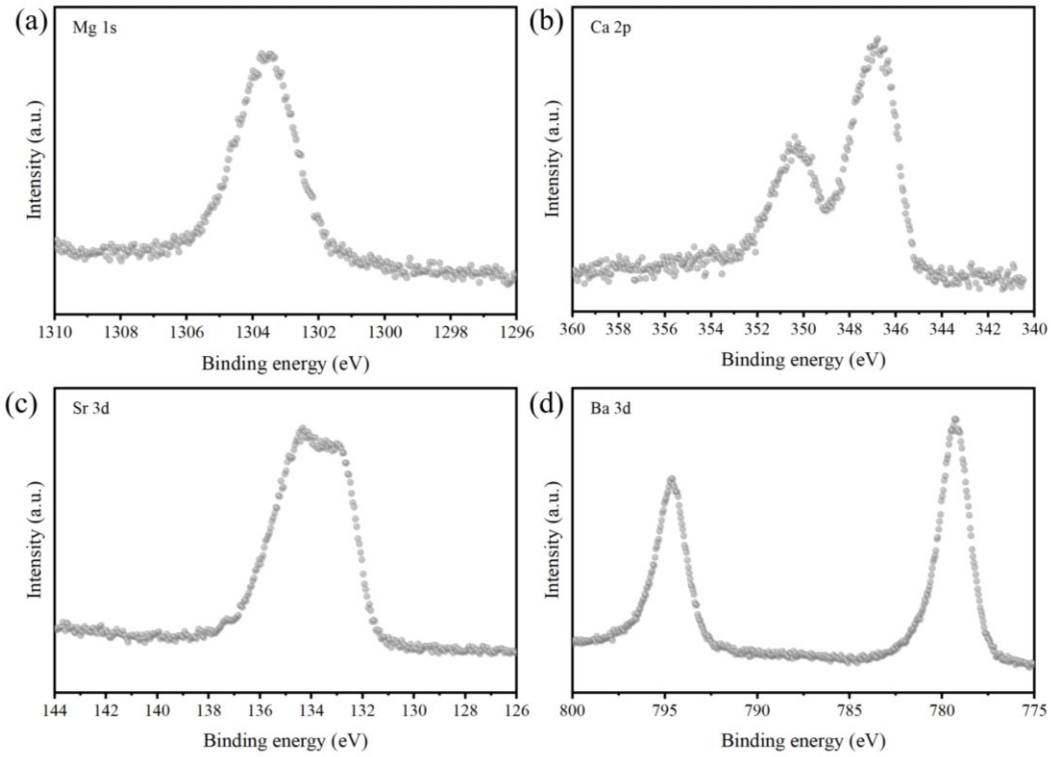

Fig. S1. XPS spectra of Mg 1s (a), Ca 2p (b), Sr 3d (c) and Ba 3d (d).

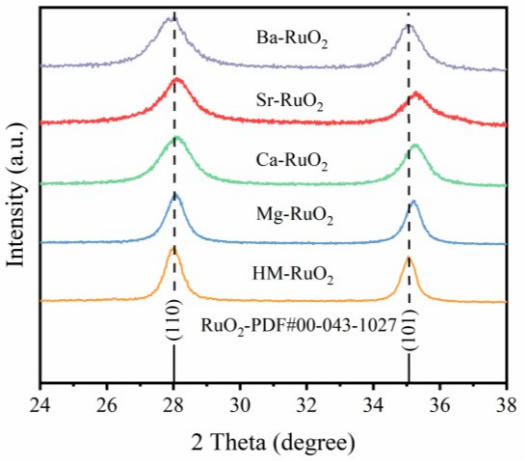

Fig. S2 Magnified XRD patterns of catalysts.

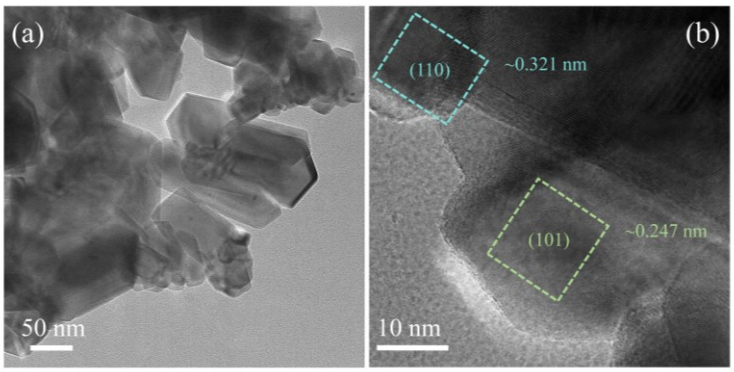

Fig. S3 TEM (a) and HRTEM (b) images of HM-RuO_2.

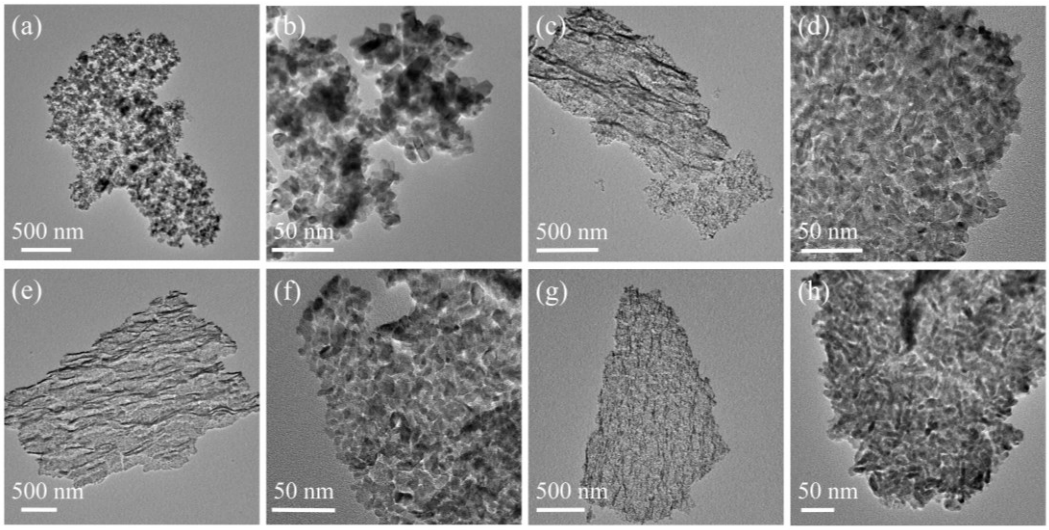

Fig. S4 TEM images of Mg-RuO_2 (a, b), Ca-RuO_2 (c, d), Sr-RuO_2 (e, f) and Ba-RuO_2 (g, h).

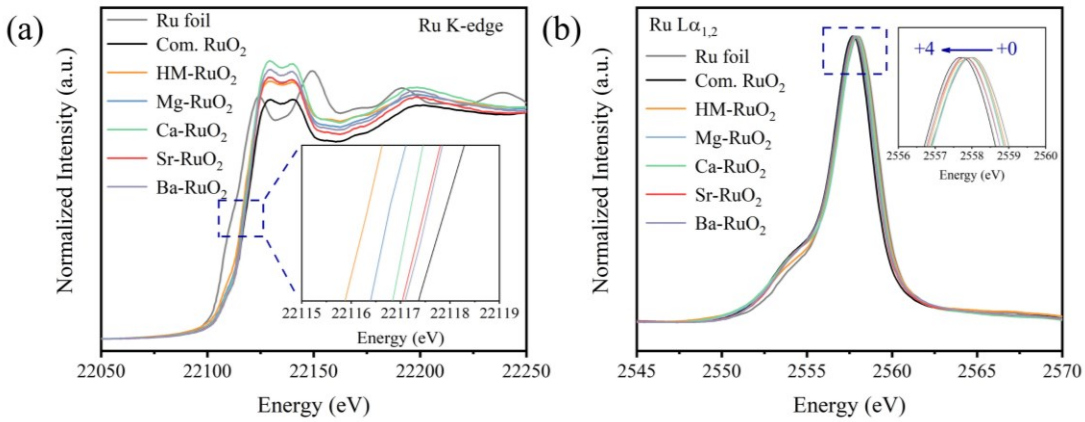

Fig. S5 (a) Normalized Ru K-edge XANES spectra of samples. (b) Normalized XES spectra of Ru $L\alpha_{1,2}$ of samples.

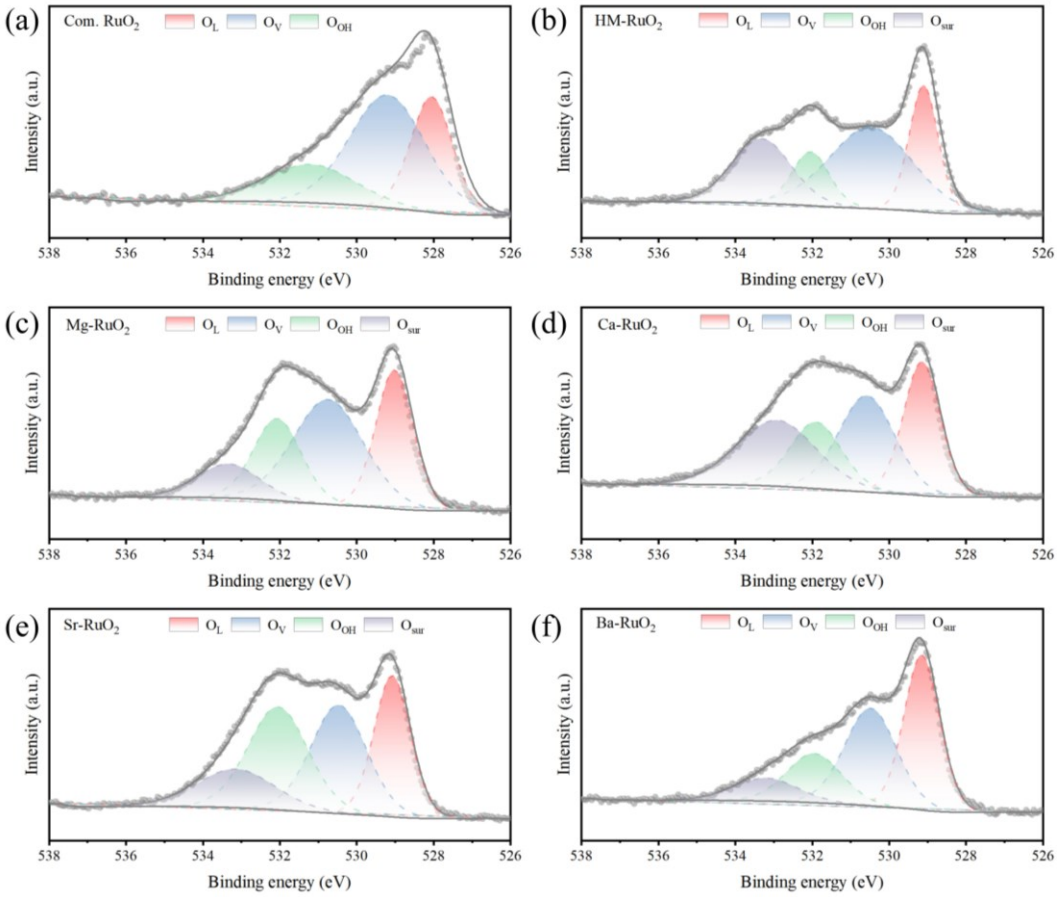

Fig. S6 O 1s spectra of Com. RuO_2 (a), HM-RuO_2 (b), Mg-RuO_2 (c), Ca-RuO_2 (d), Sr-RuO_2 (e) and Ba-RuO_2 (f).

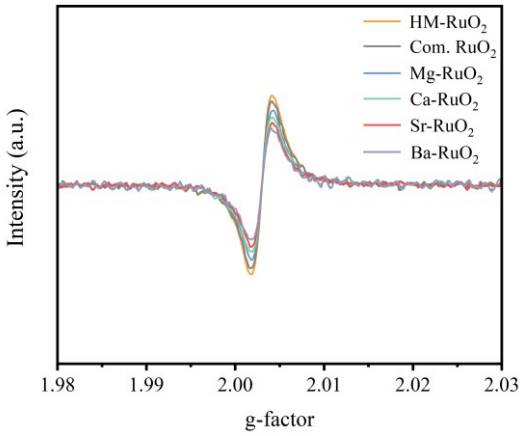

Fig. S7 EPR spectra of catalysts with different O_V densities.

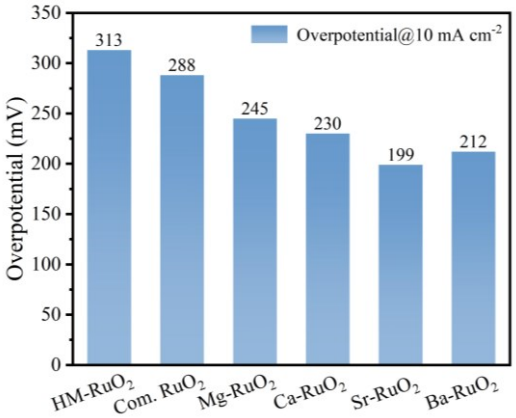

Fig. S8 Overpotential of catalysts at 10 mA cm^{-2}.

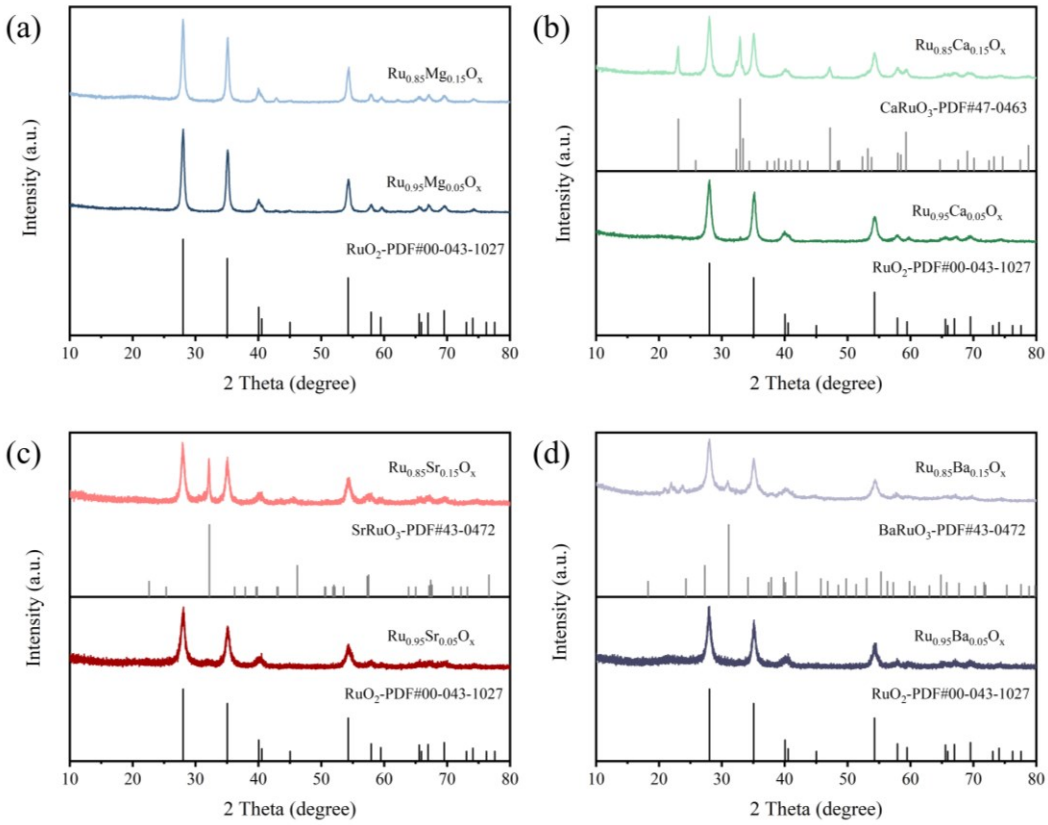

Fig. S9 (a) XRD patterns of RuO_2 catalysts with varying Mg^{2+} doping concentrations. (b) XRD patterns of RuO_2 catalysts with varying Ca^{2+} doping concentrations. (c) XRD patterns of RuO_2 catalysts with varying Sr^{2+} doping concentrations. (d) XRD patterns of RuO_2 catalysts with varying Ba^{2+} doping concentrations.

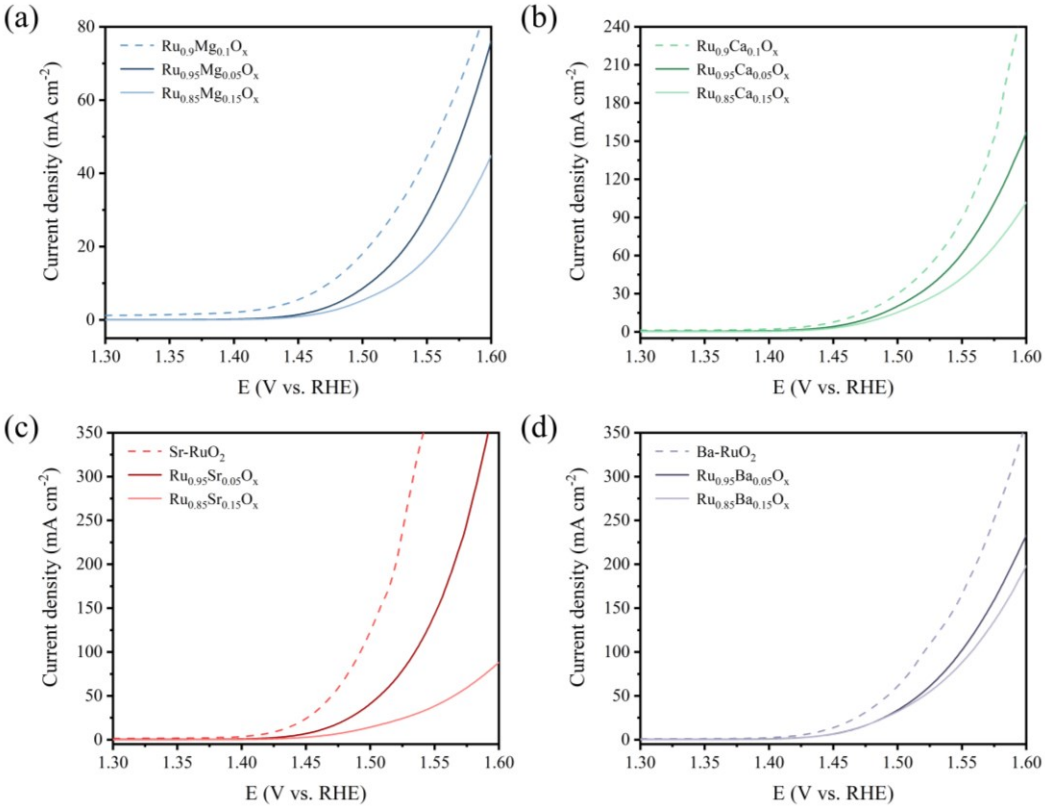

Fig. S10 (a) LSV curves of RuO_2 catalysts with varying Mg^{2+} doping concentrations. (b) LSV curves of RuO_2 catalysts with varying Ca^{2+} doping concentrations. (c) LSV curves of RuO_2 catalysts with varying Sr^{2+} doping concentrations. (d) LSV curves of RuO_2 catalysts with varying Ba^{2+} doping concentrations.

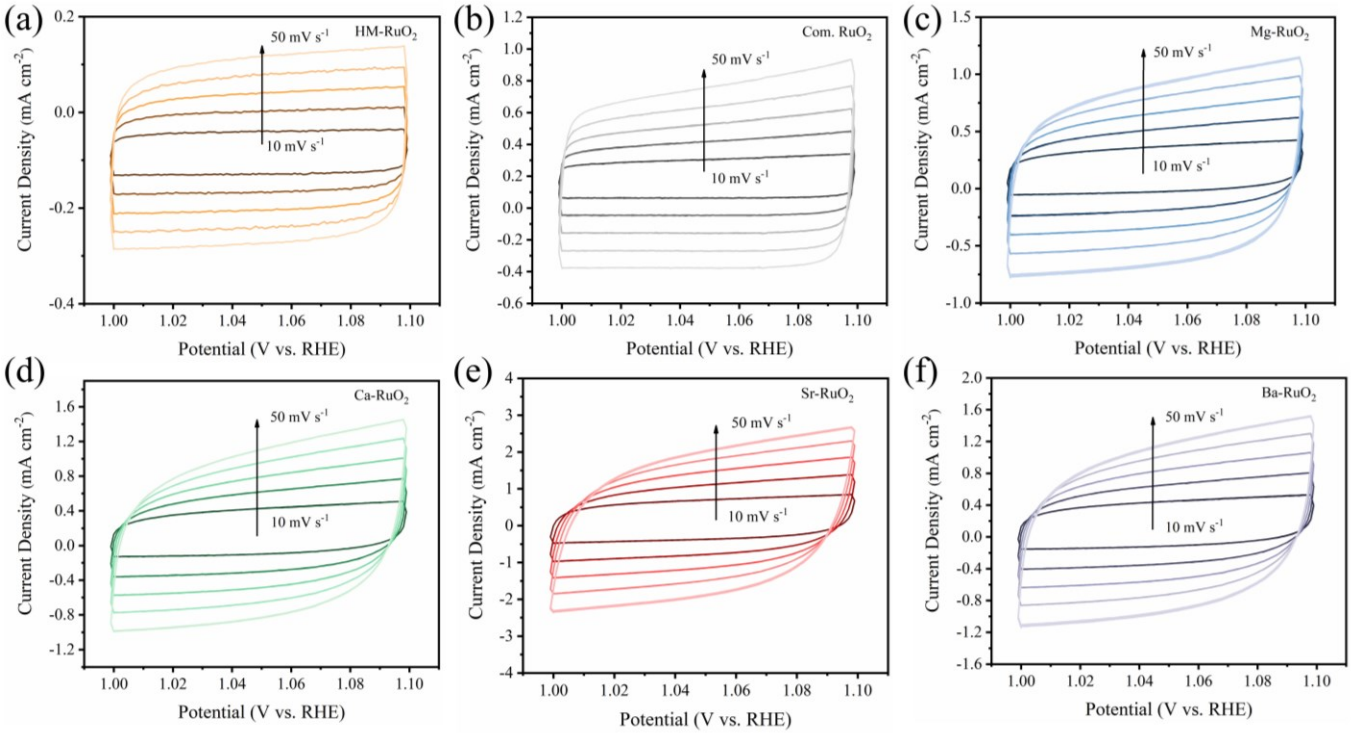

Fig. S11 CV curves from the non-reactive region for (a) HM-RuO_2, (b) Com. RuO_2, (c) Mg-RuO_2, (d) Ca-RuO_2, (e) Sr-RuO_2 and (f) Ba-RuO_2.

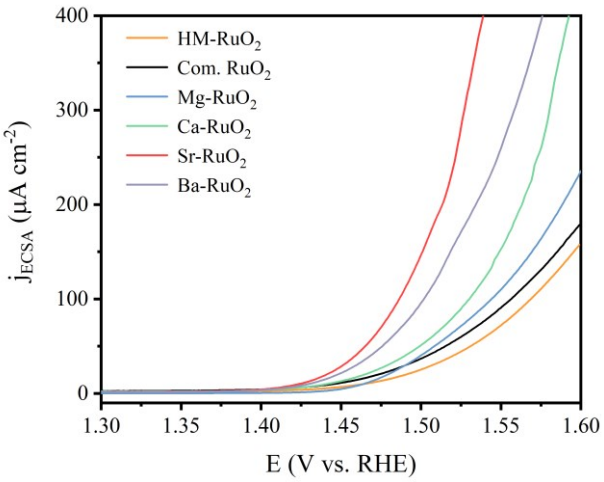

Fig. S12 OER polarization LSV curves normalized by ECSA.

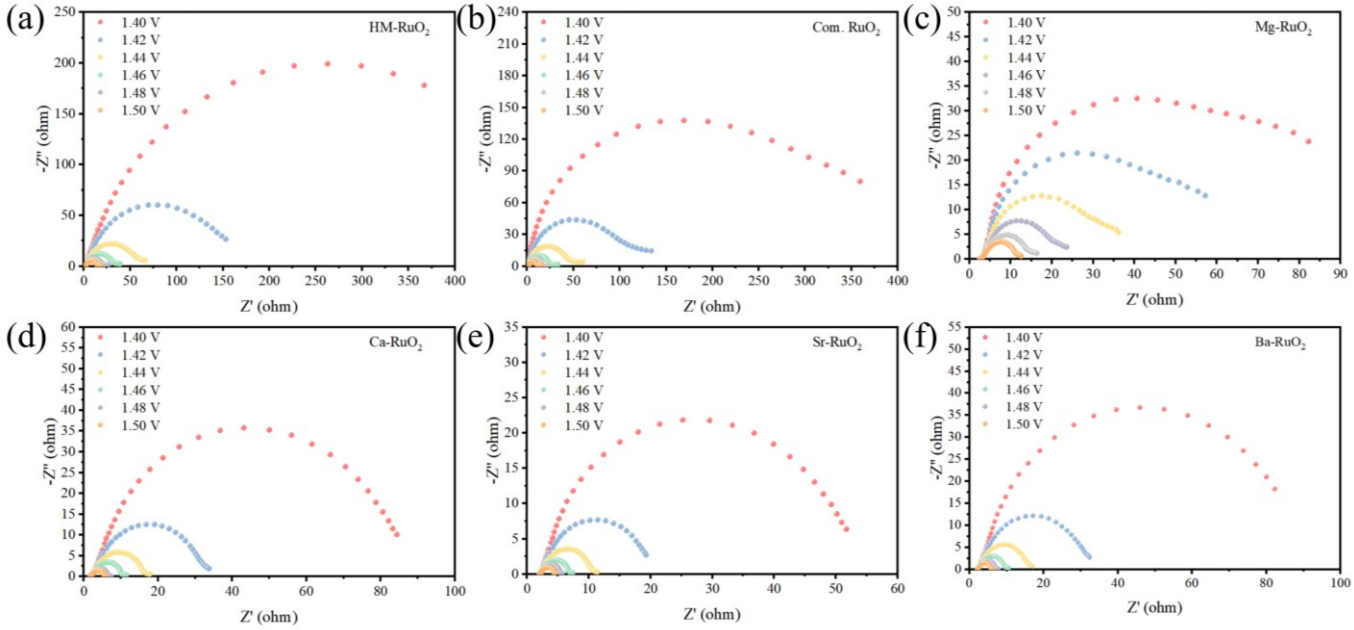

Fig. S13 Nyquist plots of catalysts from 1.40 to 1.50 V vs. RHE.

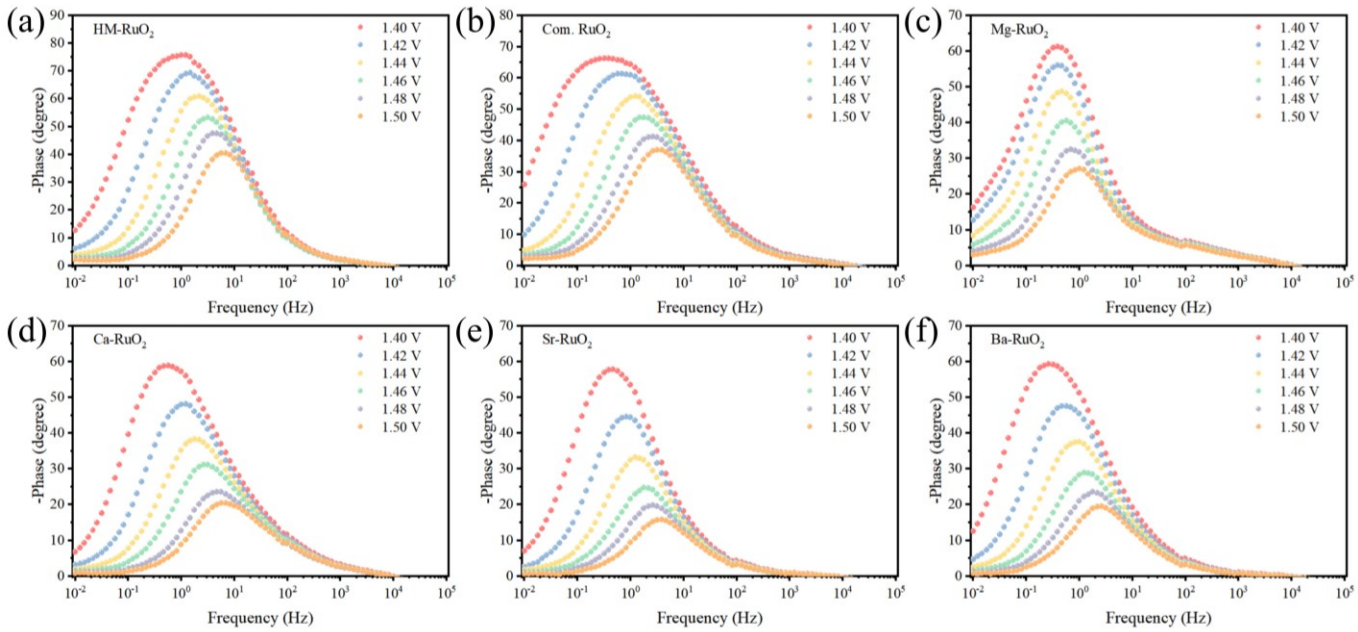

Fig. S14 Operando Bode phase plots of catalysts from 1.40 to 1.50 V vs. RHE.

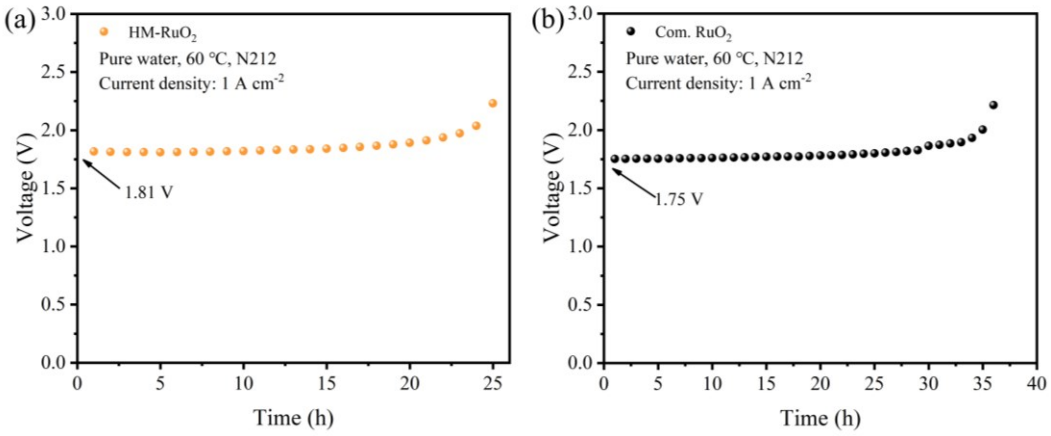

Fig. S15 Long-term durability tests at current density of 1 A cm^{-2} of HM-RuO_2 (a) and Com. RuO_2.

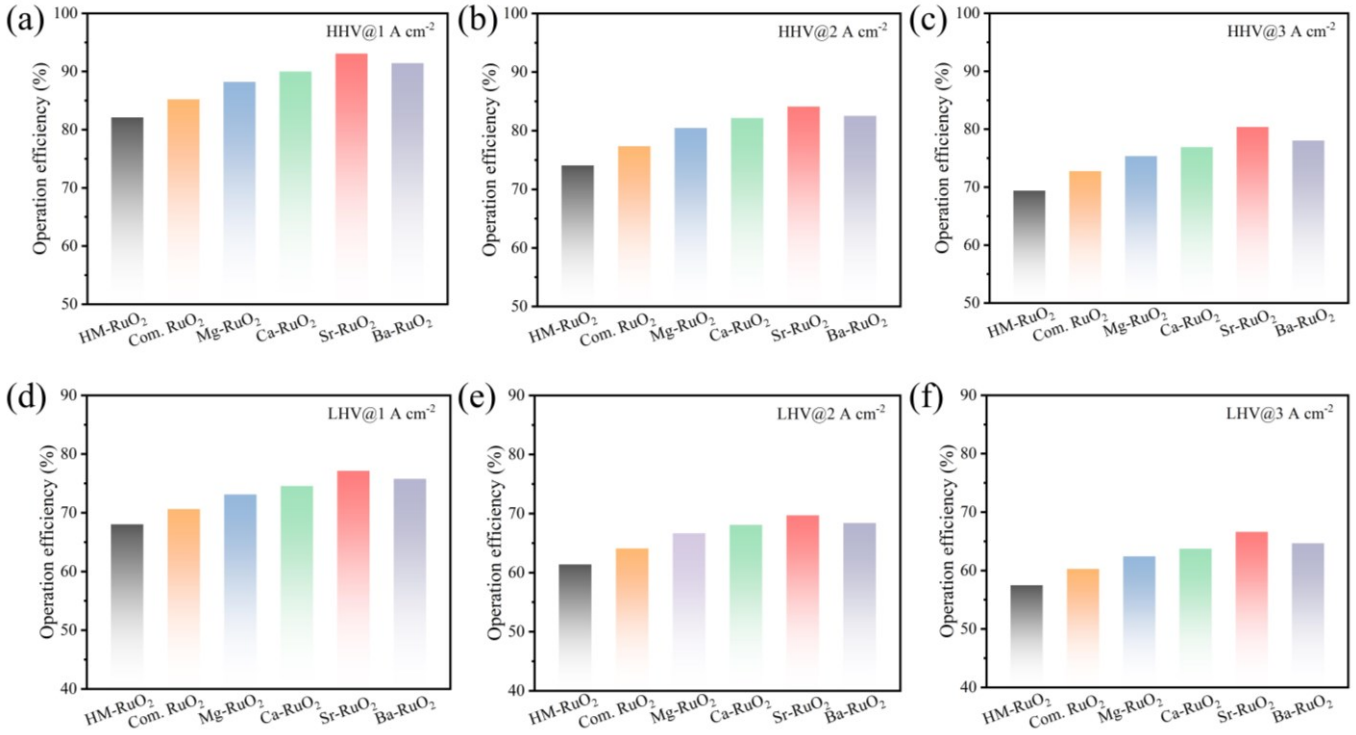

Fig. S16 The operation efficiency (calculating using higher heating value of H_2, HHV=1.43×10^5 J g^{-1}) of PEMWE utilizing HM-RuO_2, Com. RuO_2, Mg-RuO_2, Ca-RuO_2, Sr-RuO_2 and Ba-RuO_2 as the anodes at 1 A cm^{-2} (a), 2 A cm^{-2} (b) and 3 A cm^{-2} (c). The operation efficiency (calculating using lower heating value of H_2, LHV=1.185×10^5 J g^{-1}) of PEMWE utilizing HM-RuO_2, Com. RuO_2, Mg-RuO_2, Ca-RuO_2, Sr-RuO_2 and Ba-RuO_2 as the anodes at 1 A cm^{-2} (d), 2 A cm^{-2} (e) and 3 A cm^{-2} (f) [1].

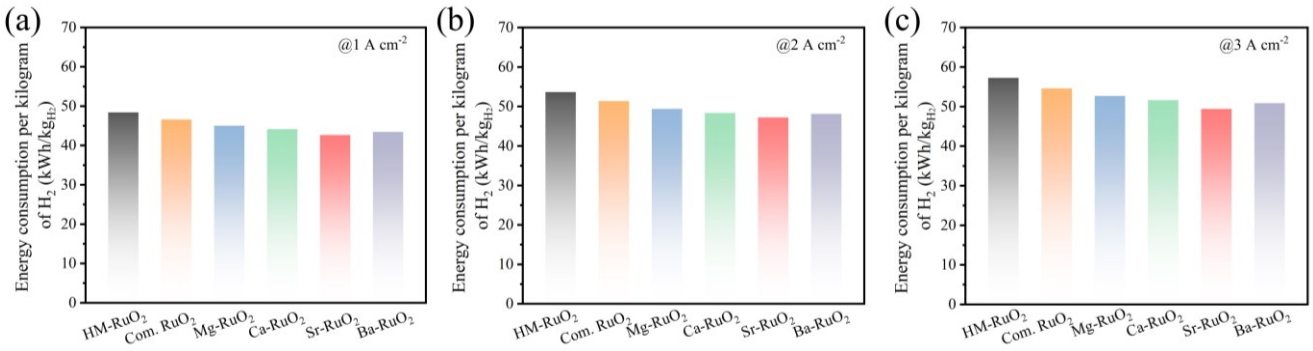

Fig. S17 The energy consumption per kilogram of H_2 for PEMWE utilizing HM-RuO_2, Com. RuO_2, Mg-RuO_2, Ca-RuO_2, Sr-RuO_2 and Ba-RuO_2 as the anodes at 1 A cm^{-2} (a), 2 A cm^{-2} (b) and 3 A cm^{-2}.

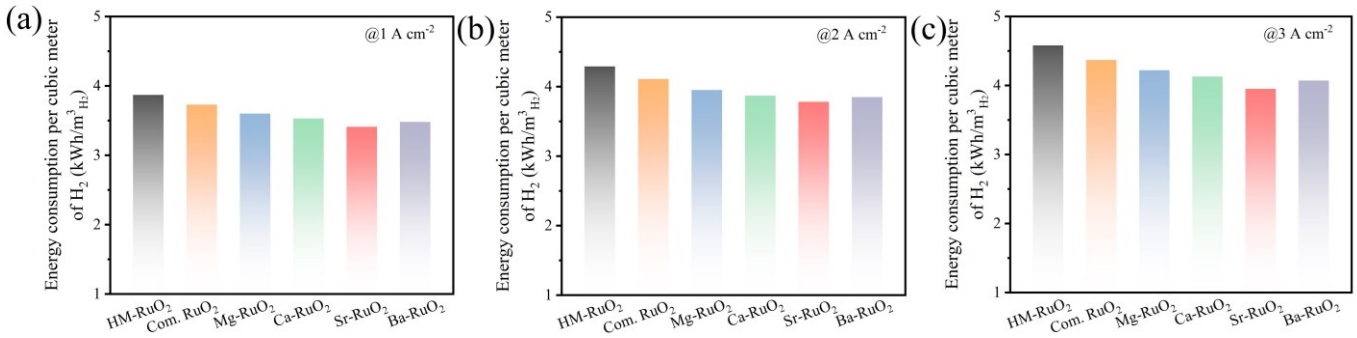

Fig. S18 The energy consumption per cubic meter of H_2 for PEMWE utilizing HM-RuO_2, Com. RuO_2, Mg-RuO_2, Ca-RuO_2, Sr-RuO_2 and Ba-RuO_2 as the anodes at 1 A cm^{-2} (a), 2 A cm^{-2} (b) and 3 A cm^{-2}.

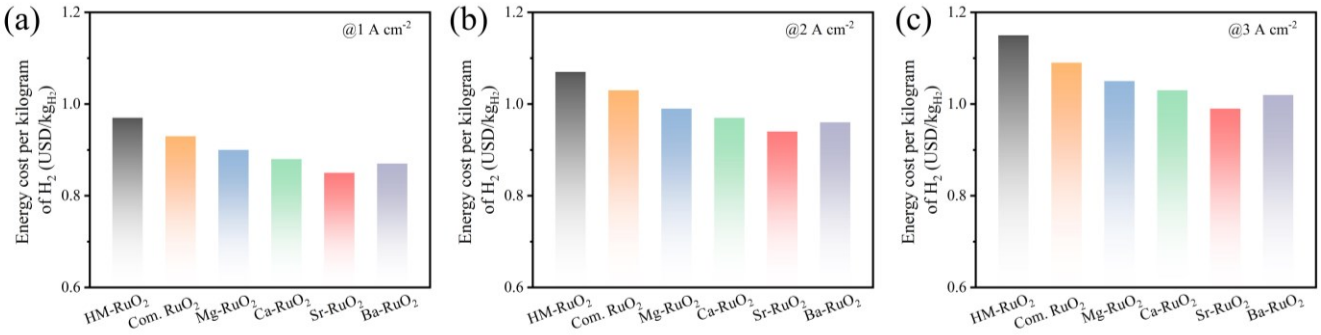

Fig. S19 The energy cost per kilogram of H_2 for PEMWE utilizing HM-RuO_2, Com. RuO_2, Mg-RuO_2, Ca-RuO_2, Sr-RuO_2 and Ba-RuO_2 as the anodes at 1 A cm^{-2} (a), 2 A cm^{-2} (b) and 3 A cm^{-2}.

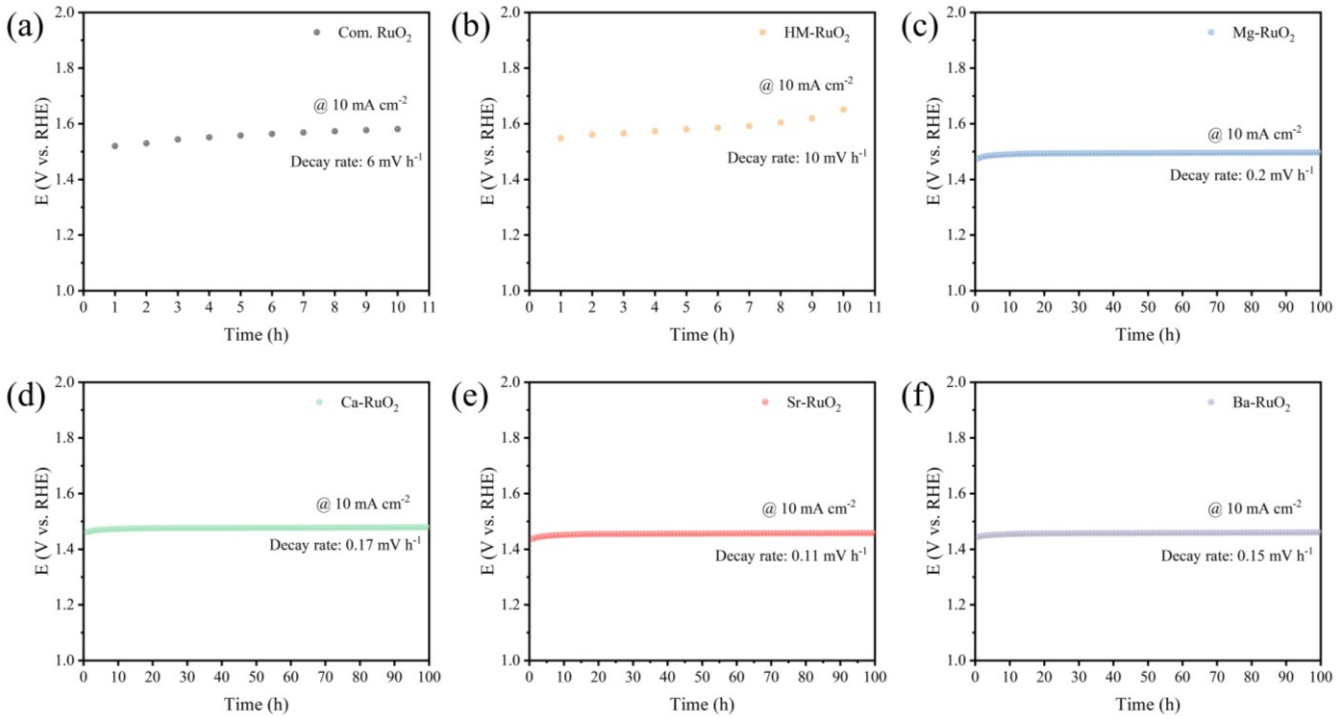

Fig. S20 Chronopotentiometric (CP) durability test at 10 mA cm^{-2}.

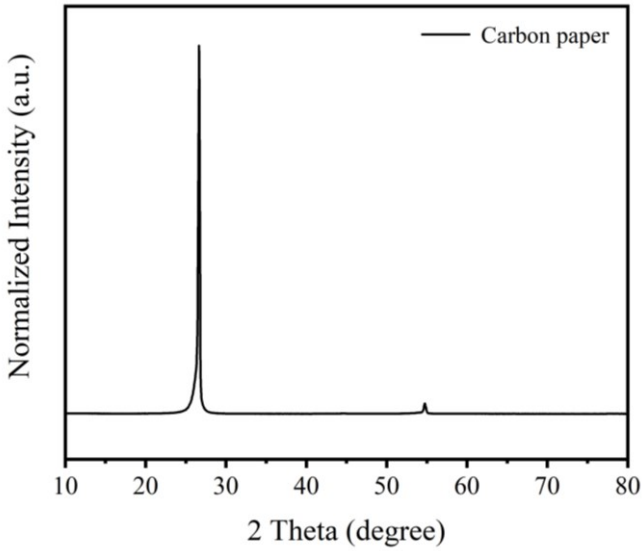

Fig. S21 XRD patterns of carbon paper.

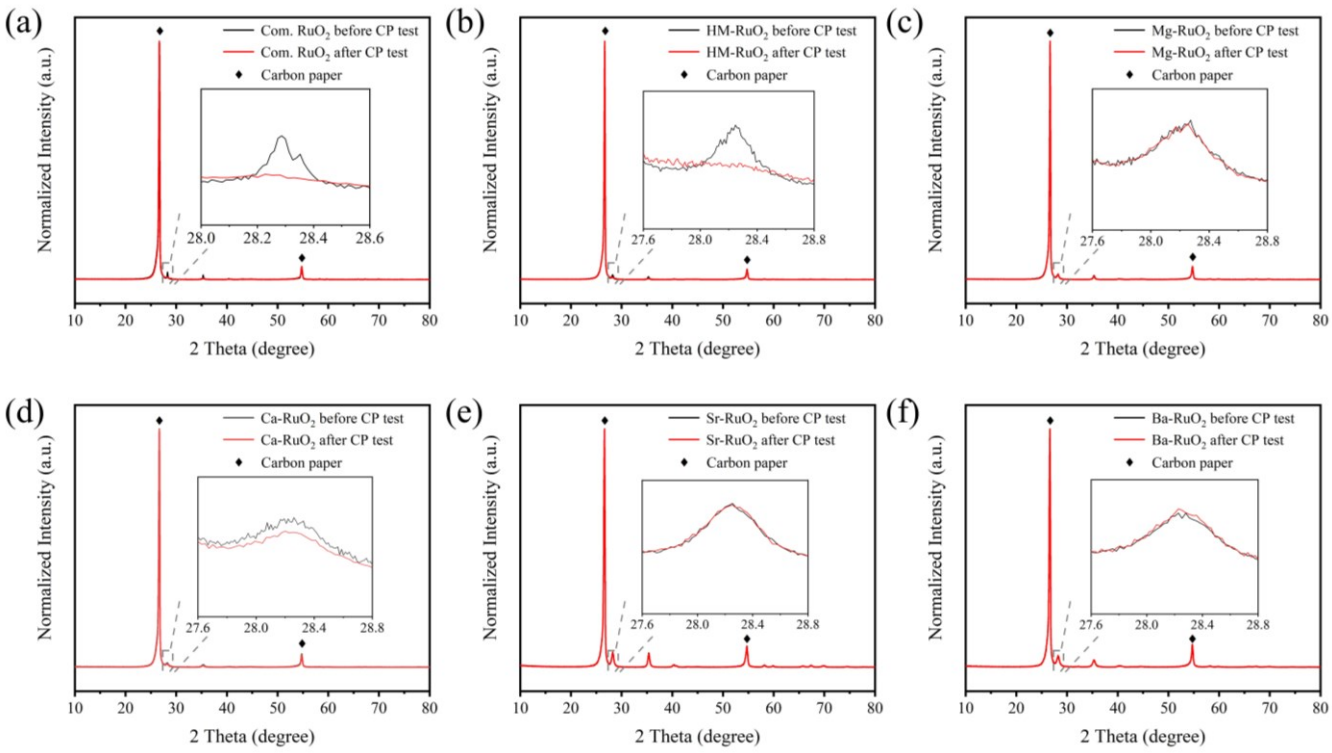

Fig. S22 XRD patterns of catalysts before and after CP tests.

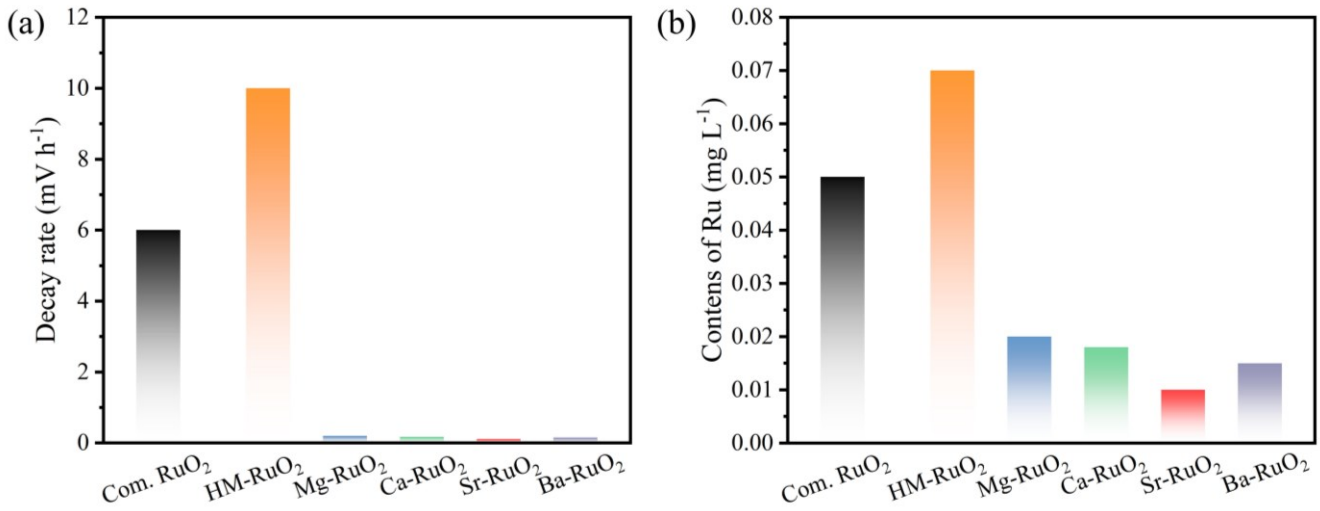

Fig. S23 (a) Decay rate of catalysts at 10 mA cm^{-2}. (b) Dependence of Ru dissolution in the electrolyte on the OER reaction time at 10 mA cm^{-2}.

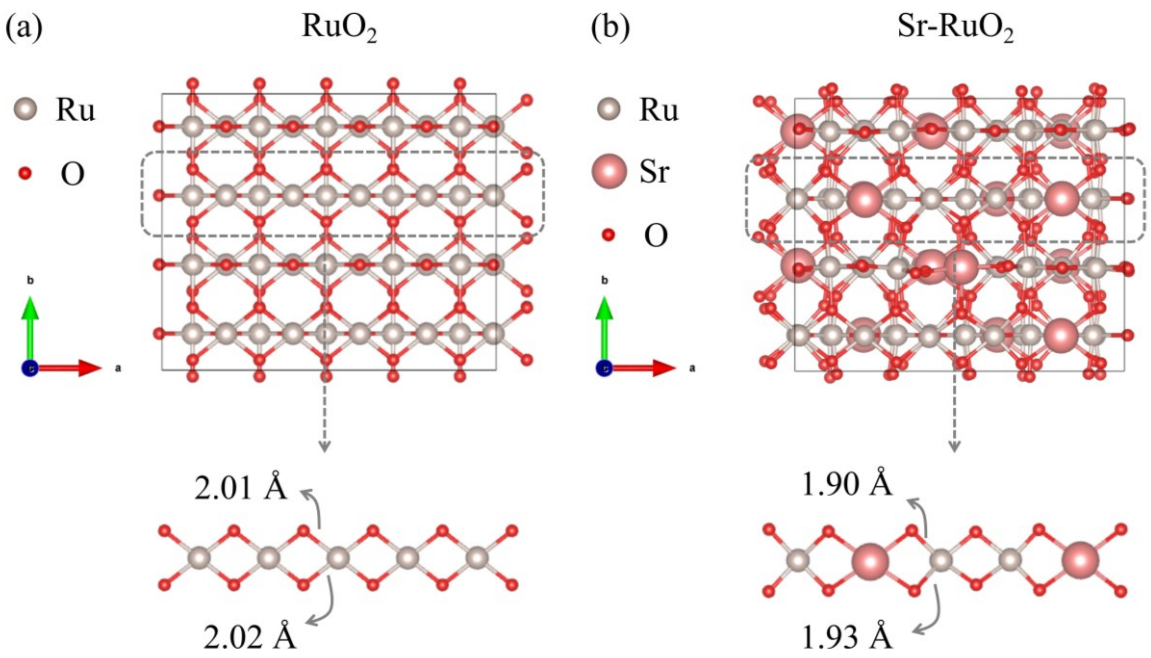

Fig. S24 Crystal structure simulation of the RuO_2 (a) and Sr-RuO_2 (b) catalysts, respectively.

Table S1. Chemical composition of the catalysts determined by ICP-OES.

Catalysts	Ru (wt%)	Ae (wt%)	Ru/Ae at. ratio
HM-RuO_2	76.32%	/	/
Mg-RuO_2	71.45%	1.92%	8.95
Ca-RuO_2	71.80%	3.15%	9.04
Sr-RuO_2	69.10%	6.61%	9.06
Ba-RuO_2	66.33%	10.04%	8.97

Table S2. Ionic radii in rutile phase.

Ion	CN	R_i/Å
Ru^{3+}	6	0.68
Ru^{4+}	6	0.62
Ru^{5+}	6	0.57
Mg^{2+}	6	0.72
Ca^{2+}	6	1.0
Sr^{2+}	6	1.18
Ba^{2+}	6	1.35

Table S3. The interplanar spacing of the catalyst.

Catalysts	(110)	(101)
HM-RuO_2	0.321	0.247
Mg-RuO_2	0.315	0.226
Ca-RuO_2	0.317	0.229
Sr-RuO_2	0.319	0.231
Ba-RuO_2	0.324	0.241

Table S4. Fitting results of O 1s XPS spectra for catalysts.

	O_L	O_V	O_{OH}	O_{sur}	O_V/O_L
Com. RuO_2	28.68%	50.82%	20.5%	/	1.77
HM-RuO_2	22.47%	41.78%	9.96%	25.79%	1.86
Mg-RuO_2	27.67%	39.83%	21.05%	11.45%	1.44
Ca-RuO_2	25.25%	29.65%	30.27%	14.82%	1.17
Sr-RuO_2	25.93%	27.48%	18.08%	28.51%	1.06
Ba-RuO_2	37.38%	34.31%	18.33%	9.98%	0.92

Table S5. PEMWE activity based on Ae^{2+}-RuO_2, Com. RuO_2, HM-RuO_2 and those previously reported catalysts.

Catalysts	Loading amount	Membrane	Cell temperature (℃)	Cell voltage (V) at 1A cm^{-2}	Stability (h)	Reference
Mg-RuO_2	2 mg cm^{-2}	Nafion 212	60 ℃	1.68	80@1 A cm^{-2}	This work
Ca-RuO_2	2 mg cm^{-2}	Nafion 212	60 ℃	1.65	110@1 A cm^{-2}	This work
Sr-RuO_2	2 mg cm^{-2}	Nafion 212	60 ℃	1.59	200@1 A cm^{-2}	This work
Ba-RuO_2	2 mg cm^{-2}	Nafion 212	60 ℃	1.62	150@1 A cm^{-2}	This work
Com. RuO_2	2 mg cm^{-2}	Nafion 212	60 ℃	1.74	35@1 A cm^{-2}	This work
HM-RuO_2	2 mg cm^{-2}	Nafion 212	60 ℃	1.81	25@1 A cm^{-2}	This work
LD-B/RuO_2	2 mg cm^{-2}	Nafion 117	80 ℃	1.63	300@0.25 A cm^{-2}	Ref. 2
Ir-RuO_2	3 mg cm^{-2}	Nafion 115	80 ℃	1.60	300@1 A cm^{-2}	Ref. 3
MD-RuO_2-BN	1 mg cm^{-2}	Nafion 115	80 ℃	1.64	50@1 A cm^{-2}	Ref. 4
$Cr_{0.2}Ru_{0.8}O_{2-x}$	3 mg cm^{-2}	Nafion 115	60 ℃	1.77	200@1 A cm^{-2}	Ref. 5
$RuTiO_x$	1 mg cm^{-2}	Nafion 117	80 ℃	1.60	100@0.5 A cm^{-2}	Ref. 6
GB-RuO_2	1 mg cm^{-2}	Nafion 117	80 ℃	1.54	100@0.1 A cm^{-2}	Ref. 7
Er-RuO_x	3 mg cm^{-2}	Nafion 117	80 ℃	1.59	100@1 A cm^{-2}	Ref. 8
Pb-RuO_2	1 mg cm^{-2}	Nafion 212	80 ℃	1.68	250@0.5 A cm^{-2}	Ref. 9
4f-Nd-RuO_2	2 mg cm^{-2}	Nafion 115	60 ℃	2.38	200@0.1 A cm^{-2}	Ref. 10
$Ba_{0.3}(SO_4)_\delta W_{0.2}Ru_{0.5}O_{2-\delta}$	3 mg cm^{-2}	Nafion 115	80 ℃	1.68	300@0.5 A cm^{-2}	Ref. 11

Table S6. The power and efficiency of the PEMWE by the Ae^{2+}-RuO_2, Com. RuO_2 and HM-RuO_2 as anodic catalyst at different current densities.

Anodic catalyst	Current density (A cm^{-2})	Efficiency (HHV)	Efficiency (LHV)	Energy consumption (kWh/kg H_2)	Energy consumption (kWh/m^3 H_2)	Energy cost per kilogram of H_2 (USD/kg H_2)
Mg-RuO_2	1	88.22%	73.11%	45.02	3.6	0.9
	2	80.46%	66.68%	49.37	3.95	0.99
	3	75.35%	62.44%	52.72	4.22	1.05
Ca-RuO_2	1	89.99%	74.57%	44.14	3.53	0.88
	2	82.16%	68.08%	48.34	3.87	0.97
	3	76.91%	63.74%	51.64	4.13	1.03
Sr-RuO_2	1	93.09%	77.14%	42.67	3.41	0.85
	2	84.12%	69.71%	47.22	3.78	0.94
	3	80.39%	66.62%	49.41	3.95	0.99
Ba-RuO_2	1	91.43%	75.77%	43.44	3.48	0.87
	2	82.54%	68.4%	48.12	3.85	0.96
	3	78.04%	64.67%	50.9	4.07	1.02
Com. RuO_2	1	85.23%	70.63%	46.61	3.73	0.93
	2	77.35%	64.1%	51.35	4.11	1.03
	3	72.75%	60.28%	54.6	4.37	1.09
HM-RuO_2	1	82.11%	68.04%	48.38	3.87	0.97
	2	74.07%	61.38%	53.63	4.29	1.07
	3	69.37%	57.48%	57.26	4.58	1.15

References

1 D. Wang, F. Lin, H. Luo, J. Zhou, W. Zhang, L. Li, Y. Wei, Q. Zhang, L. Gu, Y. Wang, M. Luo, F. Lv and S. Guo, *Nat. Commun.*, 2025, **16**, 181.

2 G. Chen, R. Lu, C. Ma, X. Zhang, Z. Wang, Y. Xiong and Y. Han, *Angew. Chem. Int. Edit.*, 2024, **63**, e202411603.

3 H. Wu, J. Chang, J. Yu, S. Wang, Z. Hu, G. I. N. Waterhouse, X. Yong, Z. Tang, J. Chang and S. Lu, *Nat. Commun.*, 2024, **15**, 10315.

4 D. Chen, R. Yu, K. Yu, R. Lu, H. Zhao, J. Jiao, Y. Yao, J. Zhu, J. Wu and S. Mu, *Nat. Commun.*, 2024, **15**, 3928.

5 Y. Shen, X. Zhang, M. Qu, J. Ma, S. Zhu, Y. Min, M. Gao and S. Yu, *Nat. Commun.*, 2024, **15**, 7861.

6 W. Hu, B. Huang, M. Sun, J. Du, Y. Hai, W. Yin, X. Wang, W. Gao, C. Zhao, Y. Yue, Z. Li and C. Li, *Adv. Mater.*, 2025, **37**, 2411709.

7 W. He, X. Tan, Y. Guo, Y. Xiao, H. Cui and C. Wang, *Angew. Chem. Int. Edit.*, 2024, **136**, e202405798.

8 L. Li, G. Zhang, C. Zhou, F. Lv, Y. Tan, Y. Han, H. Luo, D. Wang, Y. Liu, C. Shang, L. Zeng, Q. Huang, R. Zeng, N. Ye, M. Luo and S. Guo, *Nat. Commun.*, 2024, **15**, 4974.

9 C. Zhou, L. Li, Z. Dong, F. Lv, H. Guo, K. Wang, M. Li, Z. Qian, N. Ye, Z. Lin, M. Luo and S. Guo, *Nat. Commun.*, 2024, **15**, 9774.

10 X. Zhang, Y. Zhang, B. O. Protsenko, M. A. Soldatov, J. Zhang, C. Yang, S. Bo, H. Wang, X. Chen, C. Wang, W. Cheng and Q. Liu, *Nat. Commun.*, 2025, **16**, 6921.

11 Y. Xue, J. Zhao, L. Huang, Y. Lu, A. Malek, G. Gao, Z. Zhuang, D. Wang, C. T. Yavuz and X. Lu, *Nat. Commun.*, 2023, **14**, 8093.